





The histone H3-lysine 4-methyltransferase Mll4 regulates the development of growth hormone-releasing hormone-producing neurons in the mouse hypothalamus

Christian Huisman¹, Young A. Kim², Shin Jeon³, Bongjin Shin³, Jeonghoon Choi¹, Su Jeong Lim ⁴, Sung Min Youn ⁴, Younjung Park³, Medha K. C.³, Sangsoo Kim⁴, Soo-Kyung Lee³, Seunghee Lee ²✉ & Jae W. Lee ³✉

In humans, inactivating mutations in *MLL4*, which encodes a histone H3-lysine 4-methyltransferase, lead to Kabuki syndrome (KS). While dwarfism is a cardinal feature of KS, the underlying etiology remains unclear. Here we report that Mll4 regulates the development of growth hormone-releasing hormone (GHRH)-producing neurons in the mouse hypothalamus. Our two *Mll4* mutant mouse models exhibit dwarfism phenotype and impairment of the developmental programs for GHRH-neurons. Our ChIP-seq analysis reveals that, in the developing mouse hypothalamus, Mll4 interacts with the transcription factor Nrf1 to trigger the expression of GHRH-neuronal genes. Interestingly, the deficiency of *Mll4* results in a marked reduction of histone marks of active transcription, while treatment with the histone deacetylase inhibitor AR-42 rescues the histone mark signature and restores GHRH-neuronal production in *Mll4* mutant mice. Our results suggest that the developmental dysregulation of Mll4-directed epigenetic control of transcription plays a role in the development of GHRH-neurons and dwarfism phenotype in mice.

¹Department of Pediatrics, Oregon Health and Science University, Portland, OR, USA. ²College of Pharmacy and Research Institute of Pharmaceutical Sciences, Seoul National University, Seoul, Korea. ³Department of Biological Sciences, University at Buffalo, Buffalo, NY 142604, USA. ⁴Department of Bioinformatics and Life Science, Soongsil University, Seoul, Korea. ✉email: leeseung@snu.ac.kr; jlee269@buffalo.edu

Kabuki syndrome (KS), caused by haploinsufficiency of *MLL4* or *UTX*, is a human developmental disorder that affects multiple tissues. One of the consistent cardinal features of KS is stunted growth and postnatal short stature¹. For instance, a report on growth data in 39 KS patients revealed that postnatal growth retardation is a clinical feature in all cases². To date, however, the molecular etiology underlying stunted growth and short stature in KS patients remains ambiguous. The postnatal growth is controlled by the hypothalamus–pituitary gland–liver axis³. First, growth hormone-releasing hormone (GHRH)-neurons in the hypothalamus release GHRH, which then stimulates secretion of the growth hormone (GH) from the pituitary gland. GH, in turn, induces the expression of insulin-like growth factor 1 (IGF1) in the liver, which controls bone epiphyses, muscle and adipose tissue development, growth plates development, and glucose homeostasis⁴. It is noteworthy that all 18 genetically confirmed prepubertal KS children successfully underwent catch-up growth after receiving a year-long treatment with recombinant human growth hormone (GH)⁵. These results suggest that the deficits of human KS patients in GH signaling should involve the production of GHRH (in the hypothalamus) and/or GH (in the pituitary) but not the events downstream of the pituitary in GH signaling pathway.

GHRH neurons are located in the hypothalamic arcuate nucleus (ARC, aka ARH), which centrally regulates diverse homeostatic processes critical for survival and reproduction^{3,6–8}. The single-cell RNA-seq (scRNA-seq) analyses of the adult mouse ARC uncovered that the ARC contains as many as 24 distinct neuronal types⁹. Among these ARC neuronal types, GHRH-neurons constitute the hypothalamus–pituitary–liver regulatory axis, which directs linear growth. AgRP-neurons enhance food intake and reduce energy expenditure by releasing the neuropeptides NPY and AgRP, while POMC-neurons perform the opposite actions using the neuropeptides α MSH (cleaved from POMC) and CART⁶. Kiss1-neurons control reproduction via the *Kiss1*-encoded neuropeptide Kisspeptin, which triggers the secretion of gonadotrophin-releasing hormone (GnRH) from the hypothalamic GnRH-neurons⁸. To understand the developmental process for the ARC, we recently established gene expression profiles for each ARC neuronal type undergoing the cell fate specification and differentiation in the mouse embryonic hypothalamus and identified 83 genes that are most specifically enriched in developing GHRH-neurons relative to other developing ARC neurons¹⁰.

The genetic cause of KS has been relatively well understood. A majority of KS is caused by mutations in the *MLL4* gene, but some cases of KS are due to mutations in the *UTX* gene¹. The human genetics of KS corroborate the finding that *MLL4* and *UTX* together form a histone-modifying enzyme complex named *MLL4*-complex, which controls gene expression, often in cell type-specific manners^{11,12}. These data also strongly support the notion that the defect in *MLL4/UTX*-directed epigenetic gene regulation is a main contributing factor to human KS phenotypes. *MLL4* is a histone H3-lysine 4 (H3K4)-methyltransferase. The methylation patterns in the histone H3K4 residue form versatile epigenetic marks that are intimately linked to the induction of associated genes. The promoters are decorated by H3K4 trimethylation (H3K4me3), while the enhancers are marked by H3K4 mono- and di-methylations (H3K4me1 and H3K4me2)¹³. In lower eukaryotes, a singular H3K4-methyltransferase Set1 performs H3K4 methylations through a large steady-state Set1-complex¹³. The H3K4-methyltransferase action is divided among multiple complexes in higher eukaryotes. *Drosophila* has dSet1-, Trx-, and Trr-complexes that generate H3K4-methylation marks¹⁴. Mammals have six similar complexes, collectively named Set1-like complexes, and each complex contains one of the six H3K4-methyltransferase, Set1 α or its paralog Set1 β , MLL1 or

its paralog MLL2 (aka WBP7), or MLL3 (aka KMT2C) or its paralog MLL4 (aka KMT2D)^{11,12}. We have identified the first two mammalian Set1-like complexes, MLL3- and MLL4-complexes^{15,16}. Interestingly, among the six mammalian Set1-like complexes, only the MLL3- and MLL4-complexes contain the H3K27-demethylase UTX¹¹, which removes the transcriptionally repressive chromatin mark H3K27 methylation¹³. Thus, MLL3/4-complexes have two distinct enzymatic activities that lead to the open chromatin formation for transactivation of the target genes. Consistently, the MLL3/4-complexes function as transcriptional coactivators that trigger target gene expression, and the subunits in the MLL3/4-complexes serve as adaptors that recruit MLL3/4 and UTX to enhancers of their target genes by partnering with transcription factors bound to those enhancers^{11,12}.

With regards to MLL3/4-directed epigenetic gene regulation, the interplay between the two histone marks H3K4-methylation and H3K27-modification is noteworthy. MLL3/4 have been shown to be the main enzymes that generate the enhancer marks H3K4me1 and H3K4me2 (refs. 17–21). H3K4me1/2 marks concomitantly occur with another active enhancer mark H3K27ac, often preceding H3K27ac^{22,23}. Several studies provide the molecular basis for the co-occurrences of H3K4me1/2 and H3K27ac marks^{23–26} and suggest that MLL3/4-directed H3K4me1/2 are intimately linked to H3K27ac.

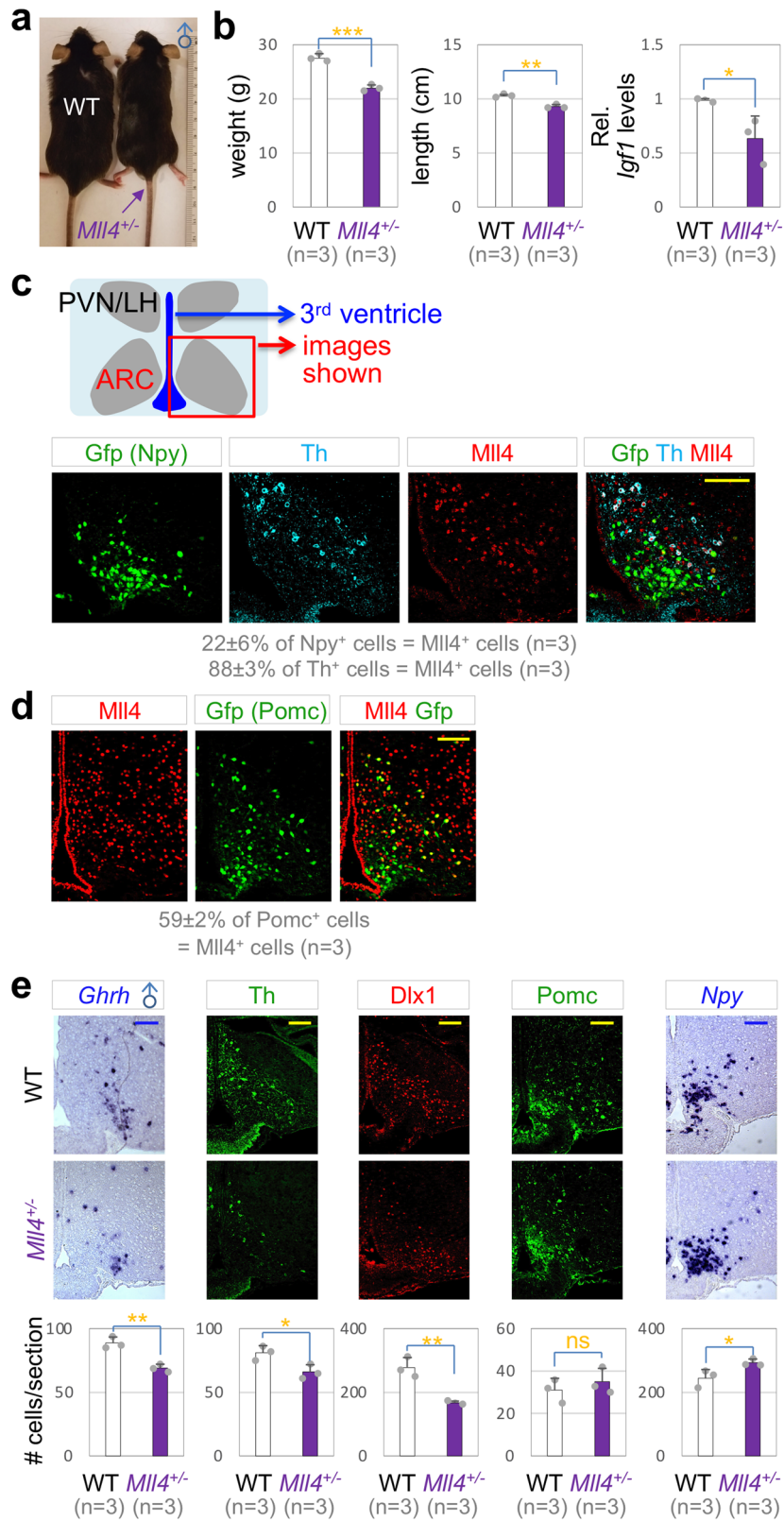
In this paper, we report that *Mll4* governs the development of GHRH-neurons in the mouse hypothalamus via its epigenetic regulatory activity. Further, we found that *Mll4* triggers the expression of GHRH-neuronal genes during development, primarily by partnering with the transcription factor Nrf1 (for nuclear respiratory factor 1, aka α -Pal). Together, our study revealed that the deficiency of *Mll4*-directed epigenetic control of GHRH-neuronal genes results in a severe reduction of GHRH neurons and dwarfism in the mouse, providing crucial insights into the molecular etiology underlying dwarfism in human KS patients.

Results

***Mll4*^{+/-} mice exhibit dwarfism and the reduction of GHRH neurons.** To test if *Mll4* haploinsufficiency leads to dwarfism in mice as it does in human, we monitored the growth of *Mll4*^{+/-} mice, in which a single *Mll4* allele is inactivated²⁷. *Mll4*^{+/-} mice showed a significant reduction in body weight, linear length, and mRNA levels for *Igf1* in the liver (Fig. 1a, b, Supplementary Fig. 1a), indicating that *Mll4*^{+/-} mice have a deficit in GH signaling and faithfully recapitulate one of the cardinal features of KS, postnatal growth deficiency¹.

To test the role of *Mll4* in hypothalamic GHRH neurons, we monitored the expression pattern of *Mll4* in the ARC. GHRH neurons are one of tyrosine hydroxylase (Th)⁺ neuronal types in the ARC²⁸. Interestingly, *Mll4* was expressed in ~88% of Th⁺ neurons that include GHRH neurons, but only in ~22% of *Npy*⁺ AgRP-neurons at postnatal day 33 (P33) in *Npy-Gfp* reporter mice that express *Gfp* in AgRP-neurons²⁹ (Fig. 1c). In contrast, *Mll4* was expressed in ~59% of *Pomc*⁺ cells in P65 *Pomc-eGfp* reporter mice³⁰ (Fig. 1d). These results indicate that most GHRH-neurons express *Mll4*, whereas only a subset of AgRP- and POMC-neurons express *Mll4*.

Next, we tested if the number of GHRH-, AgRP-, and POMC-neurons changes in *Mll4*^{+/-} mice using a panel of markers. GHRH-neurons significantly reduced, as determined by GHRH-neuronal markers, *Ghrh*, Th, and *Dlx1*, in *Mll4*^{+/-} mice relative to littermate WT control mice (Fig. 1e). In contrast, the number of POMC-neurons did not change and AgRP-neurons mildly increased in *Mll4*^{+/-} mice (Fig. 1e). Our data indicate that the generation or survival of GHRH-neurons is impaired in *Mll4*^{+/-} mice, and also suggest that the deficiency of GHRH-neurons is



likely a strong contributing factor to the dwarfism in *MII4* haploinsufficiency.

The inactivation of *MII4* in the developing hypothalamus leads to a drastic reduction of GHRH neurons and dwarfism. To test

if *MII4* plays a cell-autonomous role in GHRH-neuronal development, we generated *MII4* conditional knockout (*MII4*-cKO) mice, in which *MII4* was deleted in the embryonic ARC, by crossing *MII4*^{ff} and *Nkx2-1-Cre* mice^{21,31}. In *MII4*-cKO mice, *MII4* expression was largely eliminated in the developing ARC, but not in surrounding tissues, by embryonic day (E) 12.5

Fig. 1 Dwarfism of *Mll4*^{+/-} mice. **a** *Mll4*^{+/-} male mice are smaller than their littermate WT mice at P80. **b** A significant reduction in body weight as well as linear length and liver *Igf1* levels in male *Mll4*^{+/-} mice relative to their littermate WT mice at P80. **c, e** Coexpression of Mll4 (IHC) with either Gfp driven by *Npy-Gfp* or Th (IHC) at P33 (**c**), and with Gfp driven by *Pomc-Gfp* at P33 (**d**). **e** Expression of *Ghrh*, Th, *Dlx1*, *Pomc*, and *Npy* in the ARC of male WT mice and their littermate *Mll4*^{+/-} mice at P80, assessed by ISH (*Ghrh*, *Npy*) and IHC (Th, *Dlx1*, *POMC*). Quantifications were done by counting the number of labeled cells in three rostral to caudal sections for each mouse, and the number of mice used is as indicated in parenthesis (**c-e**). The location of ISH/IHC images is schematically shown (**c**), which applies to all images in (**c-e**). Scale bars, 100 μ m. Statistical differences were determined by two-sided Student's *t*-test (**b, e**); **p* < 0.05, ***p* < 0.01, ****p* < 0.001, and not significant (ns). Column bars represent mean, error bars indicate the SD (**b, e**).

(Fig. 2a). At E14.5~E15.5, GHRH-neurons expressing *Ghrh* and Th were markedly reduced in *Mll4*-cKO mice compared to littermate control mice (Fig. 2b, c), indicating that the development of GHRH-neurons was impaired in the absence of Mll4. *Mll4*-cKO mice also showed a striking reduction of GHRH-neurons at P65 (Fig. 2b, c), indicating that the developmental defects of GHRH-neurons in *Mll4*-cKO embryos were not recovered at adult stage. In contrast to GHRH-neurons, the number of AgRP-neurons did not significantly change in *Mll4*-cKO mice (Fig. 2d). We also tested the marker for other hypothalamic neurons; *Trh*, a marker for the dorsomedial hypothalamus that does not express *Nkx2-1*³² and *Sfl*, a marker for a subregion of the ventromedial hypothalamus that expresses *Nkx2-1*^{32,33}. Neither *Sfl*⁺ nor *Trh*⁺ cells were significantly altered in their numbers in *Mll4*-cKO mice (Supplementary Fig. 2), highlighting a relatively selective loss of GHRH-neurons in the *Mll4*-deficient hypothalamus.

To determine if the mere expression of *Ghrh* gene alone or the developmental program for GHRH-neurons was disrupted in *Mll4*-cKO mice, we examined the expression pattern of transcription factors that are crucial to drive GHRH-neuronal development. We have previously reported that *Dlx1* and its paralog *Dlx2* are required for the development of mouse Th⁺ neurons, which include GHRH-neurons³⁴ and that *Foxp2* is essential for the generation of mouse GHRH-neurons¹⁰. *Mash1*, expressed in neural progenitors in the ARC, and *Isl1*, expressed in ARC neurons, are involved in the development of multiple ARC neuronal types³⁵⁻³⁷. Interestingly, in *Mll4*-cKO mice, the number of cells co-expressing *Dlx1* and *Foxp2* was drastically reduced (Fig. 2e), but the levels of *Isl1* and *Mash1* did not significantly change (Fig. 2f, g). These results strongly suggest that the development of GHRH-neurons, rather than just the expression of *Ghrh*, is impaired in *Mll4*-cKO mice.

Next, we examined if *Mll4*-cKO mice exhibit any growth phenotypes, reflecting the developmental deficiency of GHRH-neurons. *Mll4*-cKO mice showed a marked reduction of both body weight and linear length (Fig. 3a-c). Furthermore, serum glucose levels and hepatic *Igf1* mRNA levels drastically decreased in *Mll4*-cKO mice (Fig. 3d, e), indicating deficits in the signaling of GH, downstream of GHRH. Milder but similar results were also obtained with *Mll4*-cHET (for conditional heterozygous knockout) mice (Supplementary Fig. 1b).

Together, our results establish that Mll4 is required for the proper generation of GHRH-neurons in the developing hypothalamus. Our data also clearly link the stunted growth of *Mll4* mutant mice to the impaired development of GHRH-neurons.

Nrf1 is a major partner transcription factor of Mll4 in developing hypothalamus. To determine the molecular mechanism by which Mll4 directs the development of GHRH-neurons, we defined genome-wide Mll4-binding loci in the developing hypothalamus by performing ChIP-seq in the mouse hypothalamus at E15, a time point when GHRH-neurons are being actively specified, with the ChIP-seq quality Mll4 antibody that we developed²⁷. Our ChIP-seq analyses identified 2541 Mll4-bound ChIP-seq peaks (*p* < 0.001, FDR < 10%). Interestingly, ~85.5% of Mll4 ChIP-seq peaks were located in the promoters and gene bodies

and only ~14.5% of Mll4-bound peaks were found in the intragenic regions in the developing hypothalamus (Fig. 4a). This Mll4-occupancy pattern differs from the previous finding that Mll4 is mainly enriched in the intergenic enhancer regions in the adipocytes²¹.

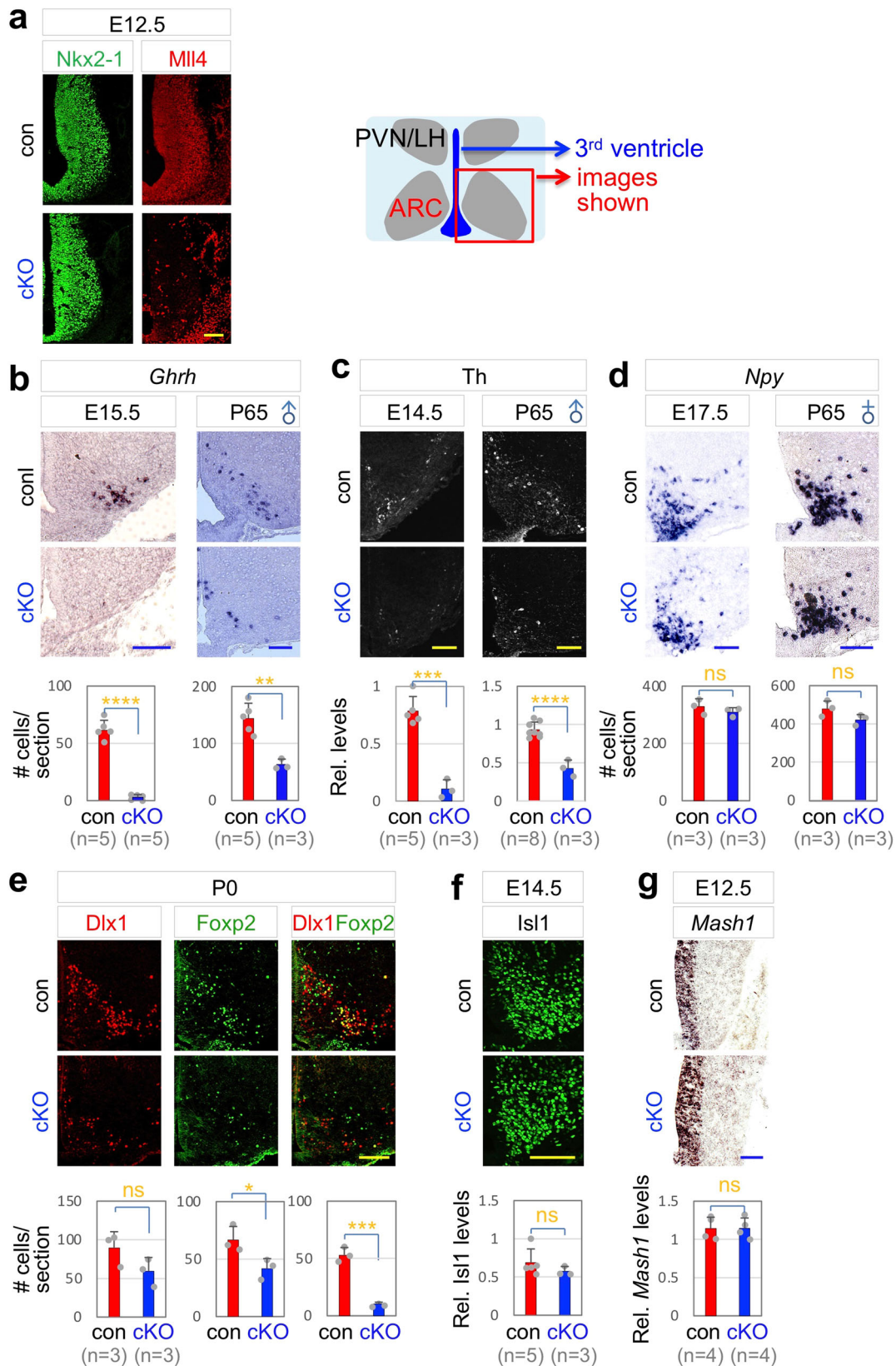
To identify partner transcription factors that mediate the recruitment of Mll4 to its target genomic loci in the developing hypothalamus, we performed de novo motif analyses on the top 300 Mll4 ChIP-seq peaks using the algorithms MEME, DREME, and TOMTOM³⁸⁻⁴⁰. Intriguingly, a single motif, which resembles the consensus binding site for the transcription factor Nrf1 (ref. 41), was found in ~92% of the top 300 Mll4 ChIP-seq peaks (Fig. 4b). The Nrf1 motif was enriched in the summit of Mll4 ChIP-seq peaks (Fig. 4c). This genome-wide analyses indicate that Nrf1 is primarily responsible for recruiting Mll4 to most Mll4-target loci in E15 developing hypothalamus.

To further test the role of Nrf1 in Mll4-directed gene regulation in the developing hypothalamus, we performed ChIP-seq in E15 hypothalamus using ChIP-seq quality Nrf1 antibody that we generated, and identified 7605 Nrf1-bound genomic regions in the developing hypothalamus (*p* < 0.001, FDR < 10%). Similar to Mll4, Nrf1 primarily occupied the promoters and gene bodies (Fig. 4d). De novo motif analyses uncovered that ~99% of Nrf1-bound genomic regions contain the Nrf1 motif (Fig. 4e). Validating that the Nrf1 motif is the binding site for Nrf1, the motif was enriched in the summit of Nrf1 ChIP-seq peaks (Fig. 4f). The direct comparison of genome-wide binding patterns of Mll4 and Nrf1 revealed that 73% of Mll4 ChIP-seq peaks are also the binding sites for Nrf1 (Fig. 4g). These data suggest that Nrf1 mediates the recruitment of Mll4 to a majority of Mll4-target genes in the developing hypothalamus (Fig. 4g). Further supporting this notion, Mll4 associated with Nrf1 in HEK293 cells, as determined by co-immunoprecipitation (coIP) assays (Fig. 4h).

Notably, Mll4 and Nrf1 co-occupied the promoter of the *Nrf1* gene itself (Fig. 4i), raising the possibility that Nrf1 auto-regulates its own transcription by recruiting Mll4 as a transcriptional coactivator. Indeed, the ectopic expression of Nrf1 enhanced the transcriptional activity of the Nrf1/Mll4-binding region in the *Nrf1* gene in HEK293 cells, as monitored using luciferase reporter assays (Fig. 4j). The expression of Nrf1 was severely reduced in the ARC region of *Mll4*-cKO mice relative to their littermate controls at E12.5 and P0 (Fig. 4k), supporting the notion that Mll4 induces the expression of Nrf1 by binding the *Nrf1* gene in the developing hypothalamus (Fig. 4l).

Together, these results suggest that, in the developing hypothalamus, Mll4 employs Nrf1 as the major partner transcription factor to bind and induce its 'direct' target genes. Given that Mll4 activates the expression of Nrf1, Mll4 is also expected to positively regulate the genes bound by Nrf1 alone without Mll4, which represent 'indirect' target genes of Mll4 (Fig. 4l).

Mll4 positively regulates GHRH-neuronal genes in the developing hypothalamus. To identify Mll4/Nrf1-target genes that are important in GHRH-neuronal development, we integrated Mll4



and Nrf1 ChIP-seq datasets with our scRNA-seq analyses of E15 ARC neurons, which revealed 83 genes that are most specifically enriched in developing GHRH-neurons relative to other ARC neuronal types¹⁰. Among the 83 genes, 7 genes recruit both Mll4 and Nrf1 to the same loci (Fig. 5a, b, Supplementary Fig. 3), suggesting that Nrf1 mobilizes Mll4 to these 7 genes thereby

activating their expression (Fig. 4). These Nrf1-Mll4-co-occupancy genes include two transcription factor genes *Prox1* and *Pbx3* and five non-transcription factor genes, *Vat1*, *Flywch2*, *Plekhg1*, *Tmem200a*, and *Them6* (Fig. 5a, b, Supplementary Fig. 3). Among the 83 genes, 24 genes including the transcription factor gene *Egr1*, are associated with the genomic regions that

Fig. 2 Ghrh expression impaired in *Mll4*-cKO mice. **a** E12.5 *Mll4*-cKO embryos show a drastic reduction in *Mll4* expression in the developing hypothalamus. Similar results were obtained from at least three independent experiments. **b-d** Expression of *Ghrh* (**b**) and *Th* (**c**), but not *Npy* (**d**), is significantly reduced in *Mll4*-cKO at both embryonic and adult stages. **e** Cells expressing *Dlx1* or *Foxp2* only as well as *Dlx1*/*Foxp2* double-positive cells are reduced in P0 *Mll4*-cKO pups relative to their littermate P0 control pups. **f, g** Expression of *Isl1* (**f**) and *Mash1* (**g**) was not significantly different between control embryos and their littermate *Mll4*-cKO embryos. The location of ISH/IHC images is schematically shown (**a**), which applies to all images in (**a-g**). Scale bars, 100 μ m. Quantifications were done by counting the number of labeled cells or the relative intensity of signals in three rostral to caudal sections for each mouse. The number of mice used is as indicated below each genotype in parenthesis (**b-g**). Statistical differences were determined by two-sided Student's *t*-test (**b-g**); * $p < 0.05$, ** $p < 0.01$, *** $p < 0.001$, **** $p < 0.0001$, and not significant (ns). Column bars represent mean, error bars indicate the SD (**b-g**).

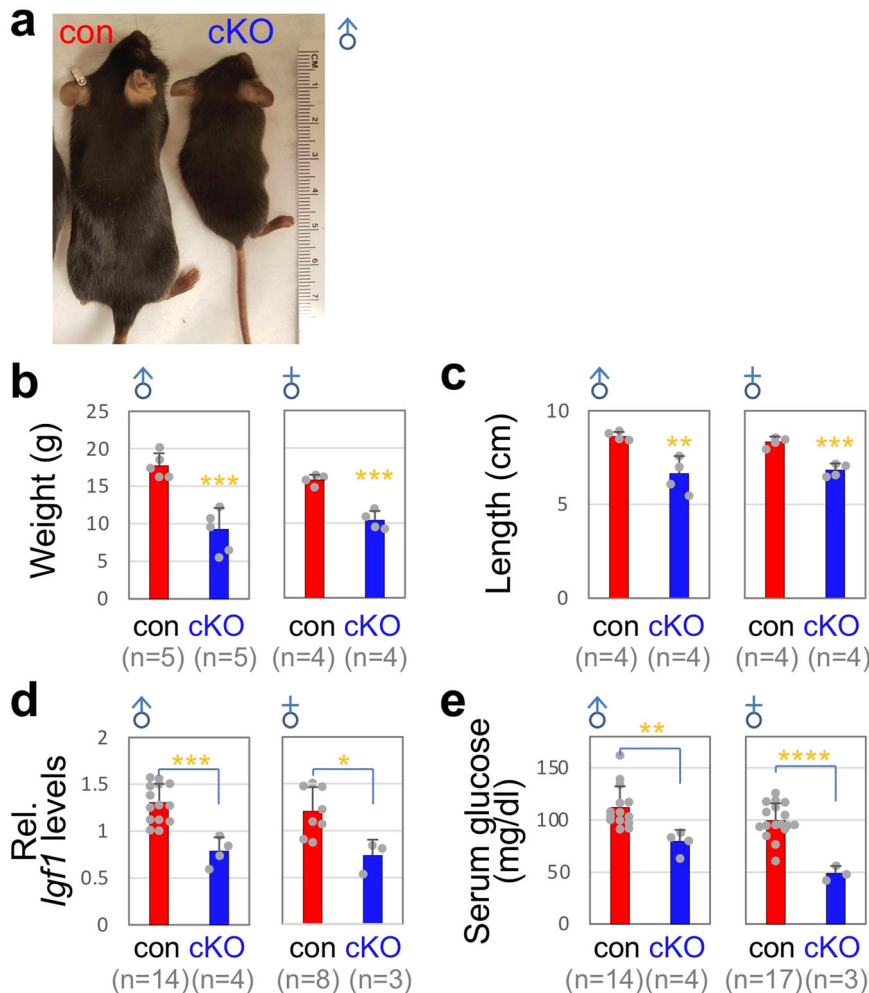


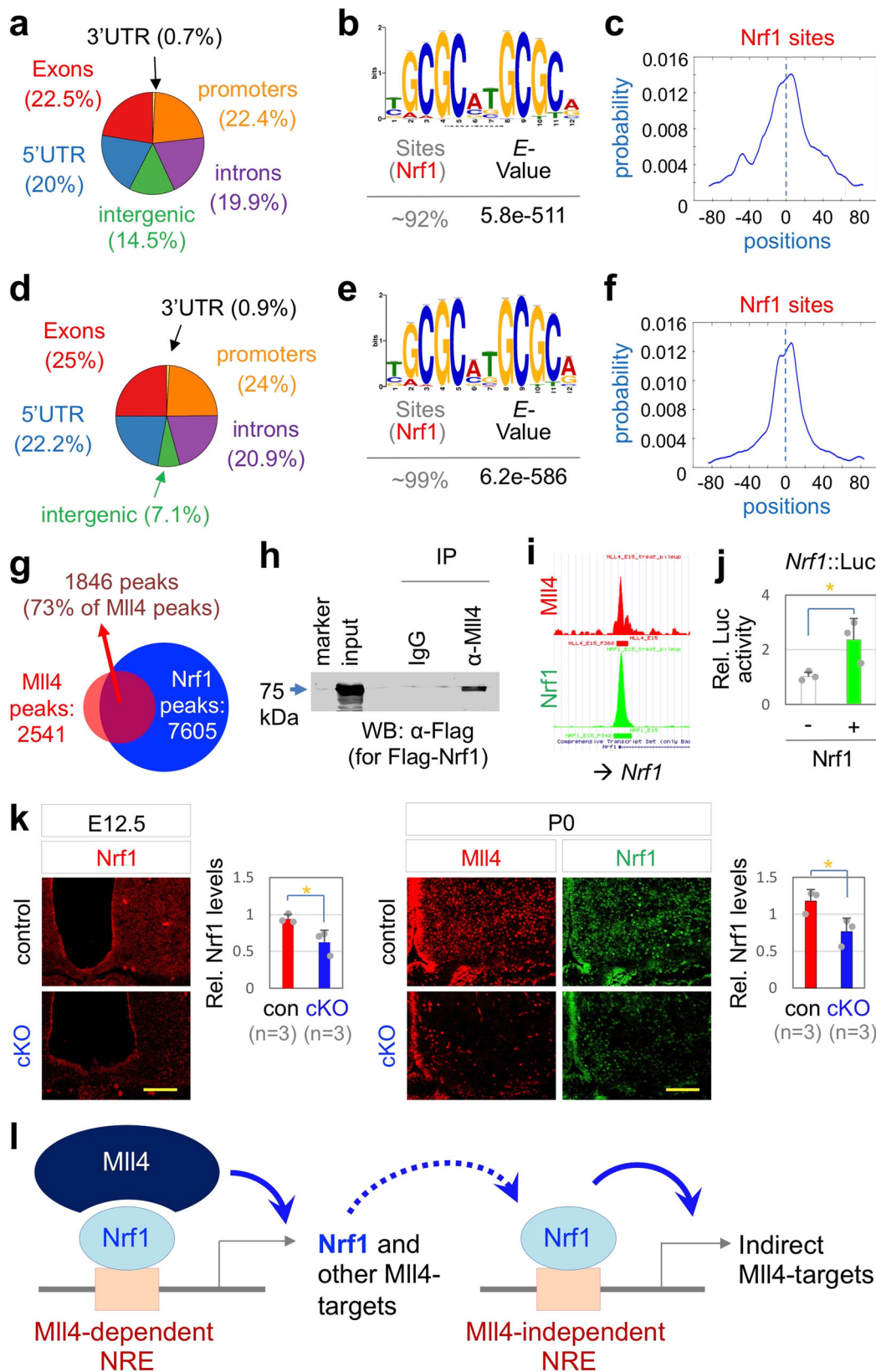
Fig. 3 Dwarfism of *Mll4*-cKO mice. **a** *Mll4*-cKO mice are smaller than their littermate control mice (a representative image for males). **b-e** A significant reduction in body weight (**b**), linear length (**c**), liver *Igf1* mRNA levels (**d**), and serum glucose levels (**e**) in male and female *Mll4*-cKO mice relative to their littermate control mice at P40. The number of mice used is as indicated below each genotype in parenthesis (**b-e**). Statistical differences were determined by two-sided Student's *t*-test; * $p < 0.05$, ** $p < 0.01$, *** $p < 0.001$, and **** $p < 0.0001$. Column bars represent mean, error bars indicate the SD (**b-e**).

recruit only *Nrf1*, not *Mll4*, thus representing potential 'indirect' *Mll4*-target genes (Fig. 4l). Interestingly, *Mll4* binds to the promoter/5'UTR of the *Dlx1* gene, but *Nrf1* does not (Fig. 5a, b), suggesting that *Mll4* induces *Dlx1* expression in the developing hypothalamus by collaborating with other transcription factor. Overall, our systematic bioinformatic analyses revealed several 'direct' and 'indirect' target genes of *Mll4* in the developing GHRH-neurons. Notably, these *Mll4*-target genes include *Dlx1*, *Prox1*, *Egr1*, and *Pbx3*, which have been shown or proposed to play a role in the development of GHRH-neurons^{10,34}.

To validate the ChIP-seq data, we performed independent ChIP assays in E15 hypothalamus using antibodies against *Mll4* and *Nrf1*. Consistent with ChIP-seq data, both *Mll4* and *Nrf1*

were recruited to the common ChIP-seq peak regions for *Mll4* and *Nrf1* regions annotated to *Prox1*, *Vat1*, *Flywch2*, and *Pbx3*, but not to the negative control genomic region *Untr6* (for Untranslated region on chromosome 6)⁴² (Fig. 5c). Also, *Nrf1* bound to ChIP-seq peak regions in *Resp18* and *Egr1*, and *Mll4* bound to *Dlx1* (Fig. 5c).

To test if *Nrf1*/*Mll4*-bound genomic genes act as enhancers responding to *Nrf1* and *Mll4*, we generated the luciferase reporters linked to *Nrf1*-*Mll4*-co-occupancy regions annotated to *Vat1* and *Flywch2*, named *Vat1::Luc* and *Flywch2::Luc*. Both luciferase reporters were activated by *Nrf1* in a dose-dependent manner and suppressed by *Mll4* knockdown with shRNA against *Mll4* in HEK293 cells (Fig. 5d), suggesting that



Nrf1 and Mll4 enhance the transcription activity of their binding regions in cells.

We predicted that the expression of the direct and indirect Mll4-target genes in mouse developing GHRH-neurons would be downregulated in the absence of Mll4. To test this idea, we examined the expression levels of potential Mll4-target genes in

the ARC of *Mll4*-cKO mice using in situ hybridization (ISH) and immunohistochemistry (IHC) analyses. *Mll4*-cKO mice showed significant downregulation of all tested target genes, such as *Pbx3* and *Plekhhg1*, which are annotated to Nrf1-Mll4-co-occupancy regions (i.e., direct Mll4-target genes), and *Pik3r1* and *Resp18*, which are associated with Nrf1 peak but not Mll4 peak

Fig. 4 *Nrf1* is a major partner transcription factor of *Mll4* in developing hypothalamus. **a–f** Location of ChIP-seq peaks in E15 hypothalamus shown for *Mll4* ChIP-seq (**a**) and *Nrf1* ChIP-seq (**d**), *Nrf1*-binding motif found in de novo motif analysis of the top 300 *Mll4* peaks (**b**) and *Nrf1* peaks (**e**), and the enrichment of the *Nrf1*-binding motif in the center of the peaks for *Mll4* (**c**) and *Nrf1* (**f**). **g** 73% of *Mll4* ChIP-seq peaks overlap with *Nrf1* ChIP-seq peaks, suggesting recruitment of *Mll4* to a majority of its targets via *Nrf1*. **h** CoIP of *Mll4* and Flag-*Nrf1* in HEK293 cells. Similar results were obtained from at least three independent experiments. **i** An identical locus of the promoter region of *Nrf1* gene is associated with *Mll4* and *Nrf1* ChIP-seq peaks. **j** A luciferase reporter construct directed by the genomic region containing the *Nrf1*-associated *Nrf1*/*Mll4*-binding locus (**i**) is activated by ectopic expression of *Nrf1* in HEK293 cells. Three independent experiments (each experiment done in duplicate) were analyzed together. **k** *Nrf1* expression is reduced in *Mll4*-cKO at both E12.5 and P0 relative to their littermate controls ($n = 3$, each genotype). Scale bars, 100 μm . Statistical differences were determined by two-sided Student's *t*-test (**j**, **k**); $*p < 0.05$. Column bars represent mean, error bars indicate the SEM (**j**) and SD (**k**). **l** A model for direct and indirect target genes of *Mll4* in the developing hypothalamus. The *Nrf1* gene is a direct target of *Mll4*:*Nrf1*, and therefore genes regulated by *Nrf1* alone can be classified as indirect target genes of *Mll4*.

(i.e., indirect *Mll4*-target genes) (Fig. 6a). While *Dlx1*, *Prox1*, and *Egr1* are highly and significantly enriched in developing GHRH-neurons, they are also expressed in other ARC neuronal types, such as the expression of *Dlx1* in developing n8/n9 TH-neurons¹⁰. Thus, to monitor the expression of *Dlx1*, *Prox1*, and *Egr1* in developing GHRH-neurons, we performed the double immunofluorescence staining with a combination of antibodies against *Dlx1* and *Prox1* or *Egr1*. *Dlx1*/*Prox1*- and *Dlx1*/*Egr1* double-positive cells in the ARC were markedly reduced in the ARC of *Mll4*-cKO mice relative to their littermate controls (Fig. 6b), indicating the downregulation of these transcription factors in GHRH-neuronal lineage and the impaired transcription program directing the development of GHRH-neurons.

Together, these studies strongly suggest that *Mll4* governs GHRH-neuronal development by inducing transcription program crucial for GHRH-neuronal differentiation and also by upregulating non-transcription factor genes that are relatively specifically enriched in developing GHRH-neurons.

***Mll4* directs GHRH-neuronal development via its epigenetic regulatory activity.** Next, to ask if *Mll4* triggers the transcriptional activation of its target genes in the GHRH-neuronal lineage via its epigenetic regulatory activity that induces transcriptionally active chromatin landscape, we sought for the method to trigger transcriptionally active chromatin, marked by H3K27ac, in *Mll4*-deficient mice. Given that the HDAC inhibitor AR-42 restored the active chromatin in the hippocampus and also rescued the hippocampal memory defects in *Mll4*^{+/-} mice⁴³, we employed AR-42. We performed daily intraperitoneal injection of 50 mg/kg of AR-42 into pregnant dams from 9 days after a vaginal plug detection until harvesting the embryos (Fig. 7a). We first monitored the active chromatin marks at E12.5. H3K4me1 and H3K4me2 levels substantially reduced in the developing ARC, but not in the surrounding tissues, in *Mll4*-cKO embryos, whereas H3K4me3 levels did not show any change (Fig. 7b, Supplementary Fig. 4a). These data suggest that *Mll4* is the main enzyme generating H3K4me1 and H3K4me2 marks in the developing ARC. Interestingly, H3K27ac levels also significantly decreased in *Mll4*-deficient ARC (Fig. 7b), consistent with the notion that enhancer marks H3K4me1/2 and H3K27ac occur concomitantly^{22,23}. AR-42 treatment restored both H3K4me1/2 and H3K27ac levels in E12.5 *Mll4*-cKO embryos (Fig. 7b). To monitor the epigenetic modification in individual *Mll4*-target genomic regions in the developing hypothalamus, we performed ChIP with antibodies against H3K4me1/2 and H3K27ac in E15 hypothalamus isolated from *Mll4*-cKO and littermate control mice following the treatment with AR-42 or vehicle. H3K4me1/2 and H3K27ac levels in *Mll4*-target loci reduced in *Mll4*-cKO mice, which was restored by AR-42 treatment (Fig. 7c). Such chromatin mark change was not observed in the negative control genomic region *Untr6* (Fig. 7c). These results suggest that AR-42 is capable of rescuing the defective chromatin landscape caused

by *Mll4* inactivation. Remarkably, AR-42 treatment also significantly increased the number of cells expressing key GHRH-neuronal fate markers *Ghrh*, *Dlx1*, and *Th* in E17.5 *Mll4*-cKO embryos (Fig. 7b, Supplementary Fig. 4b), indicating that deficiency of GHRH-neuronal developmental program in *Mll4*-null hypothalamus was at least partially repaired by AR-42 treatment. Collectively, these data suggest that the restored active chromatin landscapes by AR-42 led to the partial rescue of GHRH-neuronal development in *Mll4*-cKO mice.

Discussion

Mutations in *MLL4* result in human developmental disorder KS, whose hallmarks include dwarfism¹. Providing important insights into the etiology for the dwarfism in KS, our studies uncovered that *Mll4* governs the development of mouse GHRH-neurons during hypothalamic development by establishing transcriptionally active chromatin landscapes in collaboration with *Nrf1* and other partner transcription factors (Fig. 8). First, the two distinct mouse models, *Mll4*^{+/-} mice, which mimic the haploinsufficiency for *MLL4* in KS, and *Mll4*-cKO mice, in which *Mll4* was inactivated in the developing hypothalamus, showed impaired GHRH-neuronal development, reduced hepatic *Igf1* levels, and stunted growth. Second, our comprehensive genome-wide ChIP-seq studies for *Mll4* and *Nrf1* uncovered that *Mll4* partners mainly with *Nrf1* to activate the expression of GHRH-neuronal genes in the developing hypothalamus. Notably, *Mll4*, and *Nrf1* collaborate to trigger the expression of the *Nrf1* gene itself, suggesting that *Mll4* indirectly controls *Nrf1* alone-occupied genes via increasing *Nrf1* levels (Fig. 8). Our studies also suggest that *Mll4* may cooperate with other transcription factors. For instance, *Mll4* may be recruited to the promoter/5' UTR region of *Dlx1* by an unknown partner transcription factor. Last, the HDAC inhibitor AR-42 restored the active chromatin marks, followed by a partially rescued GHRH-neuronal developmental program, in the ARC of *Mll4*-cKO mice.

Mll4-cKO mice showed not only a reduced number of *Ghrh*-expressing cells but also a downregulation of many genes highly enriched in developing GHRH neurons¹⁰, indicating that *Mll4* inactivation led to impaired GHRH-neuronal development, rather than just downregulation of the *Ghrh* gene. These GHRH-neuronal genes include transcription factor genes *Dlx1*, *Egr1*, *Pbx3*, and *Prox1*, which are directly bound and controlled by *Mll4* according to our ChIP-seq and subsequent analyses. Given that *Dlx1* is crucial for GHRH-neuron generation and other transcription factors are candidates for key regulators of GHRH-neuronal development^{10,34}, we propose that *Mll4* activates the central gene regulatory network for GHRH-neuronal development, thus serving as a primary epigenetic regulator for GHRH-neuronal production (Fig. 8).

The findings that KS patients respond well to recombinant human GH in catch-up growth⁵ indicate that KS patients have an intact GH signaling pathway. These studies imply that the

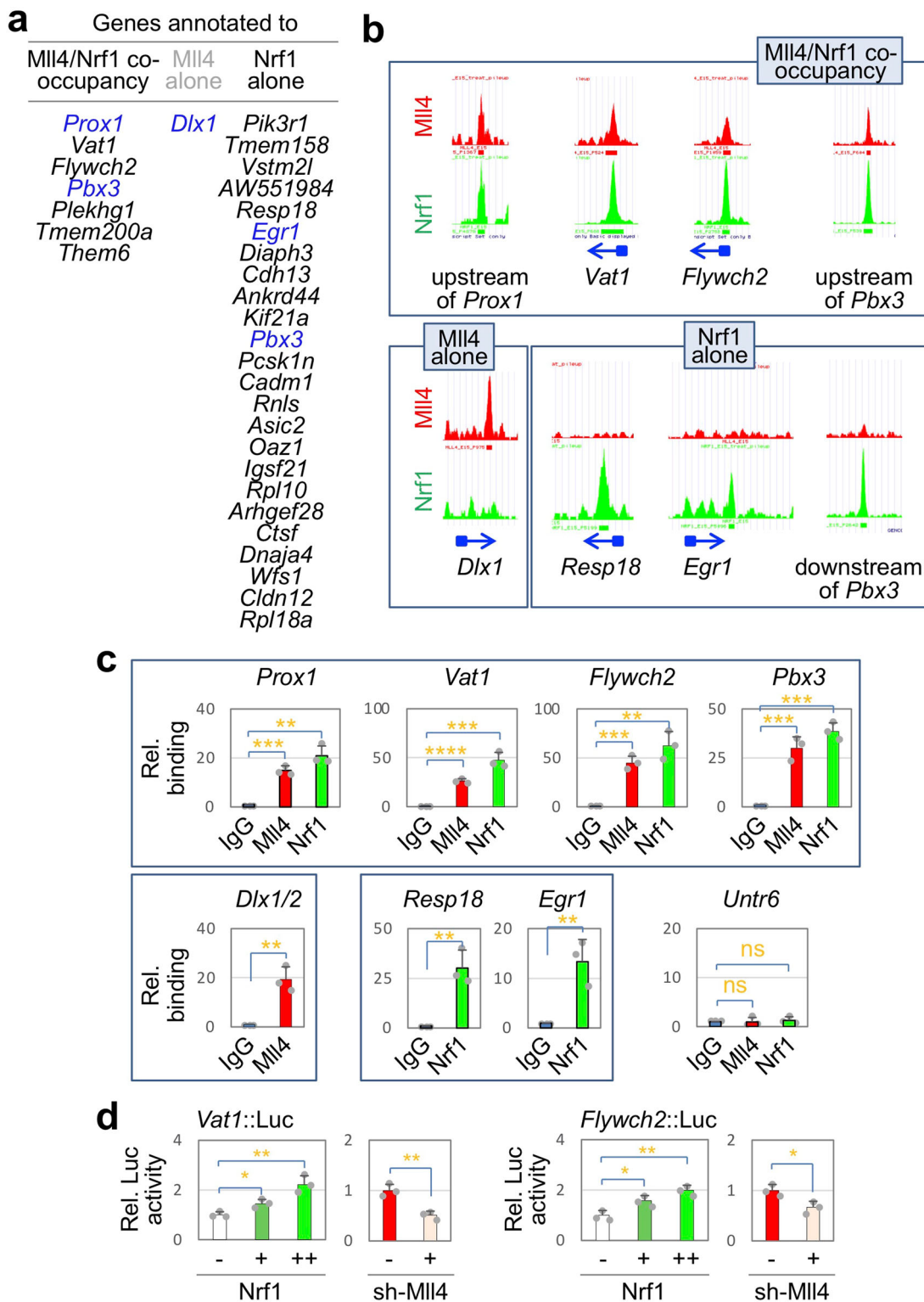


Fig. 5 Target genes of MII4 in developing mouse GHRH neurons. **a** List of genes in developing mouse GHRH-neurons, which are associated with either MII4 or Nrf1 ChIP-seq peaks or both MII4 and Nrf1 ChIP-seq peaks. Genes encoding transcription factors are highlighted in blue. **b** MII4 and Nrf1 ChIP-seq peaks for representative target genes of MII4 in developing GHRH-neurons. The location of each peak with regard to its associated gene is marked by an arrow for the direction of the gene and a square for the 5' UTR (both in blue). **c** Independent validation ChIP experiments with E15 hypothalamus and IgG (controls) and antibodies against MII4 and Nrf1 reveal recruitment of MII4 and Nrf1 to representative target genes of MII4. Column bars represent mean of experiments with three independent embryos, error bars indicate the SD. **d** Luciferase reporter assays reveal that the common ChIP-seq peak areas for MII4 and Nrf1 in *Vat1* and *Flywch2* are responsive to ectopic expression of Nrf1 and shRNA against MII4. Column bars represent mean of three independent experiments, error bars indicate the SEM. Statistical differences were determined by two-sided Student's *t*-test; not significant (ns), **p* < 0.05, ***p* < 0.01, ****p* < 0.001, and *****p* < 0.0001.

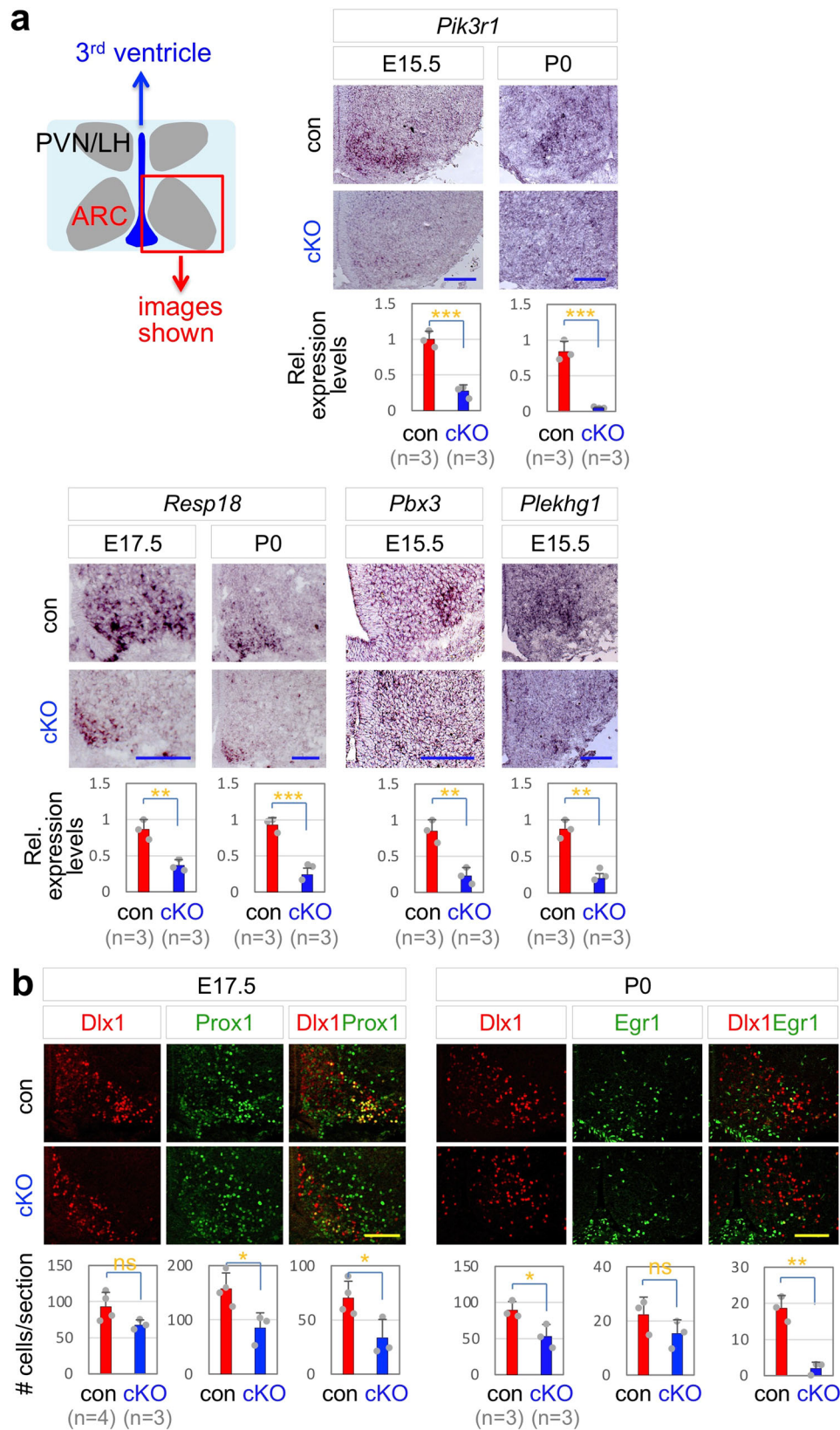


Fig. 6 *MiI4*-cKO show reduced expression of *MiI4*-target genes in developing GHRH-neurons. **a** ISH analyses of expression of *MiI4*-target genes in *MiI4*-cKO and their littermate controls at indicated stages. **b** IHC analyses of coexpression of transcription factors whose genes are targeted by *MiI4*; the number of Dlx1 only, Prox1 only, and Dlx1/Prox1 double-positive cells at E17.5, and the number of Dlx1 only, Egr1 only, and Dlx1/Egr1 double-positive cells at P0 in *MiI4*-cKO and controls. The number of mice used is as indicated below each genotype in parenthesis (**a**, **b**). The location of ISH/IHC images is schematically shown (**a**), which applies to all images in (**a**, **b**). Statistical differences were determined by two-sided Student's *t*-test; **p* < 0.05, ***p* < 0.01, and ****p* < 0.001. Column bars represent mean, error bars indicate the SD. Scale bars, 100 μ m.

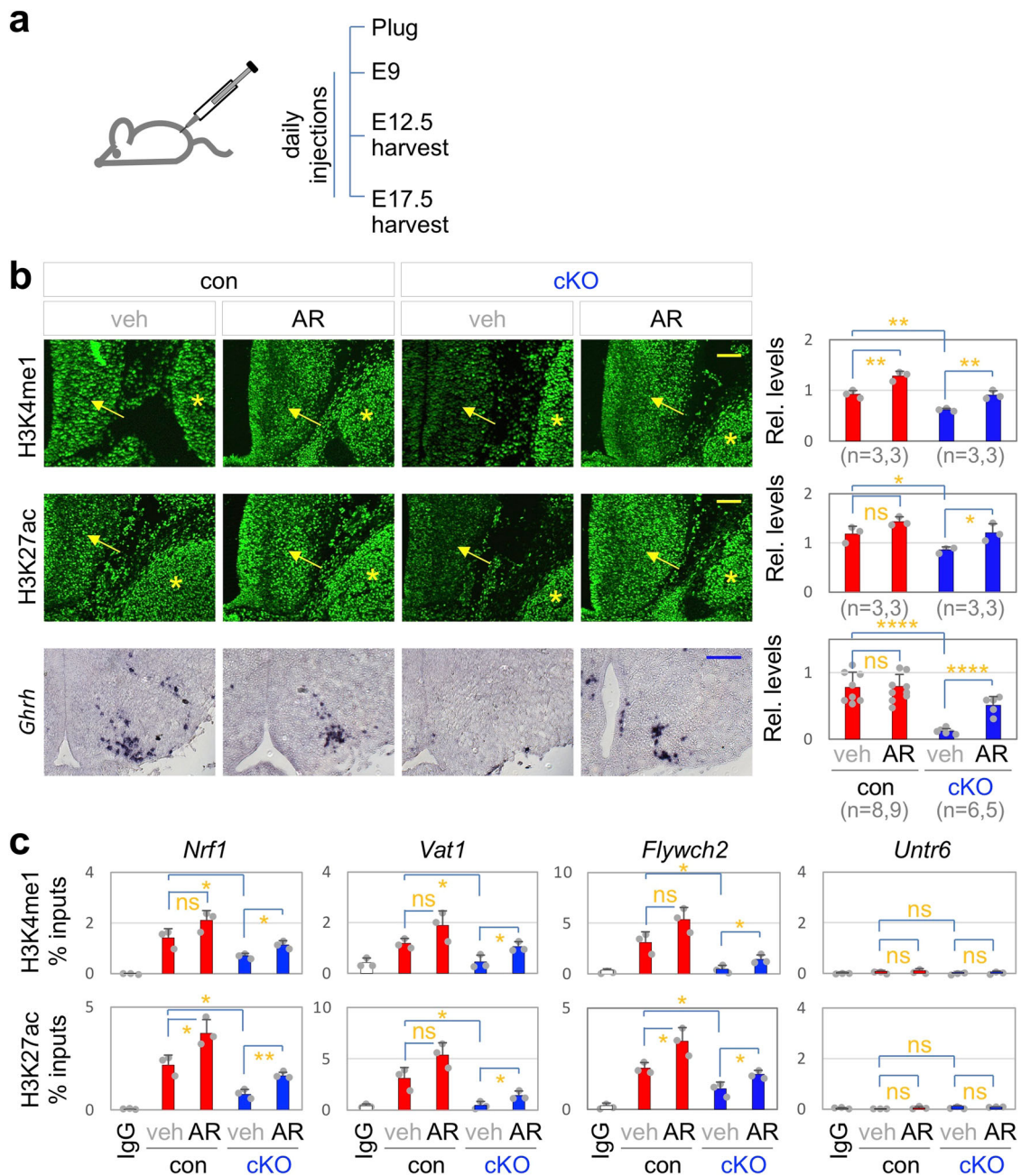


Fig. 7 AR-42 restores *Ghrh* expression in *Mll4*-cKO mice. **a** Schematics for AR-42 experiments. From 9 days after a plug was observed, vehicle or AR-42 was injected to pregnant dams daily, followed by embryo harvests at E12.5 or E17.5. **b** IHC analyses of relative levels of H3K4me1 and H3K27ac in embryos harvested at E12.5 as well as ISH analyses of *Ghrh* expression in embryos harvested at E17.5. Quantification of H3K4me1/H3K27ac levels in the developing ARC (arrows) done relative to the signals in the adjacent tissues (the trigeminal ganglion, indicated by asterisks). The number of mice used is as indicated below each genotype in parenthesis. Scale bars, 100 μ m. **c** Embryos harvested at E15 ($n = 3$, each genotype and condition) were subject to ChIP analyses with IgG (controls) or antibodies against H3K4me1 or H3K27ac, followed by qPCR quantification of H3K4me1/H3K27ac levels on genomic region containing the *Mll4*/*Nrf1* ChIP-seq peaks associated with *Nrf1*, *Vat1*, *Flywch2*, and *Untr6* (negative control locus). Statistical differences were determined by two-sided Student's *t*-test (**b, c**); * $p < 0.05$, ** $p < 0.01$, **** $p < 0.0001$, and not significant (ns). Column bars represent mean, error bars indicate the SD (**b, c**).

hypothalamus–pituitary axis producing GH is defective in KS. While our studies demonstrate an essential role of *Mll4* for the generation of GHRH neurons, it is possible that *Mll4* plays an additional role in GH production in the pituitary. In this regard, it is noteworthy that *Nkx2-1* regulates GH and prolactin transcription in the rat pituitary⁴⁴. Notably, *Nkx2-1* is also expressed in other cell types of the hypothalamus as well as forebrain and lung^{31,45,46}. Therefore, we do not exclude the possibility that the dwarfism observed with our *Mll4*-cKO mice may also involve

deletion of *Mll4* in *Nkx2-1*⁺ non-GHRH-neuronal populations in the hypothalamus or *Nkx2-1*⁺ cell types in the pituitary, fore-brain or lung, either directly or indirectly. In particular, further studies are needed to investigate the role of *Mll4* in the development and function of the pituitary, particularly regarding the pituitary production of GH.

The hippocampal memory defects of *Mll4*^{+/-} mice can be rescued by the HDAC inhibitor AR-42 or a ketogenic diet that increases the endogenous HDAC inhibitor β -hydroxybutyrate^{43,47}. Both methods

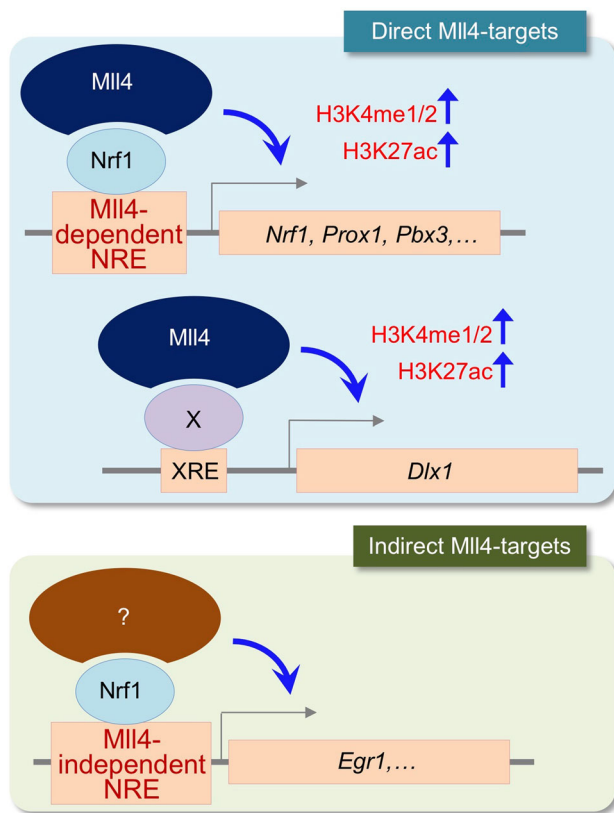


Fig. 8 Model for MLL4 action in developing GHRH-neurons. MLL4 partners mainly with Nrf1 epigenetically activating the common target genes of MLL4 and Nrf1 by enhancing the levels of H3K4me1/2 and H3K27ac. These common targets also include the *Nrf1* gene itself, resulting in indirect activation of MLL4-independent target genes of Nrf1 by MLL4 (i.e., indirect target genes of MLL4). MLL4 also partners with unknown transcription factors, for instance to activate *Dlx1*.

robustly increased H3K27ac levels^{43,47}. Here, we discovered that AR-42 also rescued the expression of *Ghrh* and other GHRH-neuronal genes impaired in the ARC of *MLL4*-cKO embryos. Notably, we wished to further test if the restored expression of *Ghrh* by AR-42 also reverses the postnatal stunted growth of *MLL4*-cKO mice, but AR-42-treated pups showed perinatal lethality to severe developmental deficits, consistent with the reported embryonic lethality of knockout mouse models for several *Hdac* genes⁴⁸. Interestingly, we found that both H3K27ac and H3K4me1 increased upon AR-42 treatment in *MLL4*-cKO mice, raising the question of which enzyme contributed to the induction of H3K4me1 in the absence of MLL4. The compensatory increase in Mll3, the paralog of Mll4, in the ARC region of *MLL4*-cKO mice (Supplementary Fig. 4c) may have been responsible for the increased H3K4me1 levels following AR-42 treatment in *MLL4*-cKO mice, which warrants future studies. Given that *MLL3* mutation has not been linked to KS or dwarfism in human, *MLL3* is unlikely to function redundantly with *MLL4* in the hypothalamus at least under normal condition.

Our results also highlight the intimate link between the two enhancer marks H3K27ac and H3K4me1/2. *MLL4* has been shown to play a role to recruit H3K27-acetyltransferases p300 and CBP to its target genes^{24–26}. Combined with these previous findings, our study suggests that *MLL4* orchestrates the establishment of transcriptionally active chromatin landscape. It remains to be addressed whether *MLL4*-directed H3K4me1/2 modification plays an active role in gene induction or simply serves as a co-occurring mark with H3K27ac. In this regard, it

will be interesting to test whether the rescue of GHRH-neuronal gene expression requires a restoration of levels of H3K27ac alone or both H3K27ac and H3K4me1/2. To this end, the chemical inhibitors of the H3K4-methyltransferase activity of MLL4 and the H3K27-acetyltransferase activity of p300 can be explored. Such inhibitors exist for p300 (ref. 49), but not for MLL4 yet. Overall, our results suggest that the missing epigenetic regulatory activity of MLL4 is the main driver for the loss of GHRH-neurons in *MLL4*-cKO mice, and further provide the proof-of-concept that *MLL4* can be a feasible target to develop epigenetic therapeutics for KS.

In summary, by combining mouse genetics, genome-wide studies, and pharmacological approaches, we demonstrated that MLL4 directs the development of mouse GHRH-neurons via its ability to modulate H3K4me1/2 and H3K27ac levels on its target genes during hypothalamus development. We also found Nrf1 as the major partner transcription factor of MLL4 in directing the development of mouse GHRH-neurons. These results strongly suggest that the dysregulation of MLL4-directed epigenetic regulation of GHRH-neuronal genes is likely a molecular etiology underlying the dwarfism in human KS patients.

Methods

Mouse work. All mice were maintained on a normal 12 h light, 12 h dark cycle with ad libitum access to chow and water, unless otherwise noted. *MLL4*^{+/−}, *MLL4*^{fl/fl}, *Pomc-Gfp*, *Npy-Gfp*, and *Nkx2-1-Cre* mice have been described previously^{21,27,29–31}. *MLL4*^{fl/fl} mice were crossed with *MLL4*^{+/−}; *Nkx2-1-Cre* mice to generate *MLL4*^{fl/fl}; *Nkx2-1-Cre* mice (*MLL4*-cKO mice). Pregnant mice were intraperitoneally injected with AR-42 (50 mg/kg, purchased from Selleck Chemicals) or vehicle (0.5% methylcellulose, 0.1% Tween-80, water) from 9 days after detecting a vaginal plug till harvest at E12.5 or E17 for analyses. All studies were approved by the Institutional Animal Care & Use Committee of University at Buffalo and Oregon Health & Science University.

Cell culture and luciferase assay. HEK293 cells were obtained from ATCC and cultured in DMEM supplemented with 10% heat-inactivated fetal bovine serum (FBS) (Thermo Scientific), penicillin/streptomycin, and L-glutamine (both Lonza). For luciferase assays, cells were seeded into 48-well plates and transfected with *Nrf1*-, *Vat1*-, or *Flywch2*-luciferase reporters and expression vectors for Nrf1 or Dlx1 or control shRNA or sh-MLL4 (ref. 27) using SuperFect (Qiagen) according to the manufacturer's instruction. Two days after transfection, luciferase activity was measured. The actin-β-galactosidase plasmid was cotransfected for normalization of the luciferase activities to transfection efficiency. Data were shown in relative luciferase units (mean ± SEM).

CoIP. For coIP, HEK293 cells were transfected with expression vector for Flag-Nrf1 using calcium phosphate transfection method. Transfected HEK293 cells were subsequently dissolved in RIPA buffer and rotated for 2 h at 4 °C. After centrifugation, the lysate was subjected to immunoprecipitation using 1 mg of Mll4 antibody o/n, followed by 2 h incubation with Protein A/G agarose beads (Thermo Fisher Scientific). Beads were then dissolved in SDS loading buffer and separated on SDS-PAGE and transferred to nitrocellulose membranes. The membranes were blocked in Odyssey blocking buffer, and incubated with primary antibodies against Flag-tag and incubated o/n. Next day, the blots were incubated with secondary antibodies, and fluorescence was detected with the Odyssey System (LI-COR), as shown in Fig. 4h (the uncropped original image in Supplementary Fig. 5).

RNA isolation and quantitative RT-PCR. Total RNA was isolated with Trizol, and converted to cDNA with a RevertAid kit (Thermo Scientific). Twenty nanograms of cDNA was used for qPCR with the ViiA7 platform and primers for amplification of *Igf1* and *Gapdh*. *Igf1* mRNA expression values were normalized to *Gapdh* using the ΔΔCt method. Relative or fold expression levels were calculated from three individual experimental replicates.

ChIP and ChIP-seq. ChIP on E15.5 hypothalamus was performed using our homemade Mll4 and Nrf1 antibodies (ref. 27 and Supplementary Fig. 6). Hypothalamus were dissected out, crosslinked for 10 min with PFA, and then quenched by 125 mM glycine. After washing in PBS, cells were lysed with lysis buffer, followed by lysis of nuclei with nuclei lysis buffer and sonification with the Pico Biorupter to generate 200–400 bp fragments. Chromatin was then 10× diluted in ChIP dilution buffer and, for immunoclearing, incubated with IgG and protein A agarose beads for 1 h. ChIP antibodies were added for o/n incubation followed by 1 h of incubation with agarose beads. Then, the beads were washed with RIPA buffer (0.1% SDS, 1% Triton X-100, 2 mM EDTA, 20 mM Tris-HCl, pH 8.0, 150 mM NaCl), high salt buffer (same components as in TSE, except 500 mM NaCl), Buffer III

(0.25 M LiCl, 1% NP-40, 1% deoxycholate, 1 mM EDTA, 10 mM Tris-HCl, pH 8.0), LIC1 buffer and TE, dissolved into TE supplemented with 10% SDS and proteinase K, incubated for 4 h at 37 °C, and decrosslinked at 65 °C o/n. DNA was subsequently isolated and subject to ChIP-seq^{50,51}.

ISH and IHC. Embryonic and P0 brains were removed and fixed in 4% PFA o/n, cryoprotected with sucrose gradients, and frozen in OCT blocks, followed by sectioning using a microtome with a thickness of 12 µm per section. P33 and P65 mice were intraperitoneally injected with Avertin before performing standard perfusion with PBS and 4% PFA, followed by fixation in 4% PFA o/n. ISH was performed at 68 °C overnight with indicated RNA probes. After hybridization, slices were incubated in washing buffer (50% formamide, 1× SSC solution, and 0.1% Tween20) for 1 h, blocked in MABT buffer + 4% BSA for 1 h, and incubated with an anti-digoxigenin-AP antibody (11093274910 Roche, 1:5000) in MABT buffer + 2% BSA. Next day, the color reaction was performed with NBP/BCIP after washing with MABT buffer. For subsequent co-staining of visualized RNA probes, hybridized sections were incubated with our homemade antibodies against Mll4 (ref. 27, 1:1000) or Dlx1³⁴ (1:1500). Next day, Vectastain ABC Elite kit (PK-6101, Vector labs) was used for the color reaction. In addition to our previously described ISH probes against *Ghrh*, *Npy*, *Trh*, *Sfl*, and *Mash1*, we also generated new RNA probes for *Pik3r1*, *Resp18*, *Pbx3*, and *Plekhg1* by converting hypothalamic RNA of P0 mice to cDNA using the primers listed in Supplementary Table 1. PCR products were then digested with the indicated enzymes and ligated into pBluescript. Digoxigenin-labeled riboprobes were generated using T7 RNA polymerase followed by purification over a column.

IHC was performed by incubating brain sections with homemade antibodies against Mll3, Mll4, Isl1, Dlx1, or Gfp (Supplementary Fig. 7) and commercial antibodies against Foxp2 (Abcam 16046, 1:2000), Prox1 (AngioBio, 1:500), Th (AB152, Millipore, 1:500), H3K4me1 (Abcam, 1:2000), H3K4me2 (Abcam, 1:1500), H3K4me3 (Abcam, 1:1000), H3K27Ac (Abcam, 1:750), Nkx2-1 (Abcam, 1:1000) in blocking buffer o/n at 4 °C. Next day, slices were washed with PBST and incubated with secondary fluorescence antibodies followed by washing and counter staining with DAPI.

Quantification and statistical analyses. For quantification of ISH/IHC images, serial sectioning was performed on embryo/mouse brain with the distance between sections 84–216 µm. One slide from each mouse that contains matched sections was used to compare controls and mutants. Zeiss Axio imager 2 with apotome was used to image ISH and IHC results. Integrated density measurement in Image J software was used to analyze densitometry. For cell counting, specifically immunostained cells in the arcuate nucleus were counted. Quantifications were done by analyzing three rostral to caudal sections for each embryo/mouse and at least three embryos/mice per each experimental group. Statistical differences were determined by two-sided Student's *t*-test. Statistical significance is displayed as follows: ns for not significant, **p* < 0.05, ***p* < 0.01, ****p* < 0.001, and *****p* < 0.0001.

Data availability

All data supporting the findings of this study are provided within the paper and its supplementary information. A source data file is provided with this paper. The ChIP-seq dataset have been deposited in GEO (GSE149439). All additional information will be made available upon reasonable request to the authors. Source data are provided with this paper.

Received: 19 March 2020; Accepted: 1 December 2020;

Published online: 11 January 2021

References

- Adam, M. P., Hudgins, L. & Hannibal, M. In *Kabuki Syndrome in Gene Reviews(R)* (eds. Pagon, R. A. et al.) (University of Washington, Seattle, 1993).
- Schott, D. A. et al. Growth pattern in Kabuki syndrome with a KMT2D mutation. *Am. J. Med. Genet. Part A* **170**, 3172–3179 (2016).
- Bluet-Pajot, M. T. et al. Growth hormone secretagogues and hypothalamic networks. *Endocrine* **14**, 1–8 (2001).
- Cohen, P. & Rosenfeld, R. G. Physiologic and clinical relevance of the insulin-like growth factor binding proteins. *Curr. Opin. Pediatr.* **6**, 462–467 (1994).
- Schott, D. A., Gerver, W. J. M. & Stumpel, C. Growth hormone therapy in children with kabuki syndrome: 1-year treatment results. *Horm. Res Paediatr.* **88**, 258–264 (2017).
- Biebermann, H., Kuhnen, P., Kleinau, G. & Krude, H. The neuroendocrine circuitry controlled by POMC, MSH, and AGRP. *Handb. Exp. Pharmacol.* 47–75 https://doi.org/10.1007/978-3-642-24716-3_3 (2012).
- Hill, J. W., Elmquist, J. K. & Elias, C. F. Hypothalamic pathways linking energy balance and reproduction. *Am. J. Physiol. Endocrinol. Metab.* **294**, E827–E832 (2008).
- Hrabovszky, E. Neuroanatomy of the human hypothalamic kisspeptin system. *Neuroendocrinology* **99**, 33–48 (2014).
- Campbell, J. N. et al. A molecular census of arcuate hypothalamus and median eminence cell types. *Nat. Neurosci.* <https://doi.org/10.1038/nn.4495> (2017).
- Huisman, C. et al. Single cell transcriptome analysis of developing arcuate nucleus neurons uncovers their key developmental regulators. *Nat. Commun.* **10**, 3696 (2019).
- Froimchuk, E., Jang, Y. & Ge, K. Histone H3 lysine 4 methyltransferase KMT2D. *Gene* **627**, 337–342 (2017).
- Lee, S., Roeder, R. G. & Lee, J. W. Roles of histone H3-lysine 4 methyltransferase complexes in NR-mediated gene transcription. *Prog. Mol. Biol. Transl. Sci.* **87**, 343–382 (2009).
- Heintzman, N. D. et al. Distinct and predictive chromatin signatures of transcriptional promoters and enhancers in the human genome. *Nat. Genet.* **39**, 311–318 (2007).
- Mohan, M. et al. The COMPASS family of H3K4 methylases in *Drosophila*. *Mol. Cell. Biol.* **31**, 4310–4318 (2011).
- Lee, S. et al. Coactivator as a target gene specificity determinant for histone H3 lysine 4 methyltransferases. *Proc. Natl. Acad. Sci. USA* **103**, 15392–15397 (2006).
- Goo, Y. H. et al. Activating signal cointegrator 2 belongs to a novel steady-state complex that contains a subset of trithorax group proteins. *Mol. Cell. Biol.* **23**, 140–149 (2003).
- Guo, C. et al. KMT2D maintains neoplastic cell proliferation and global histone H3 lysine 4 monomethylation. *Oncotarget* **4**, 2144–2153 (2013).
- Herz, H. M. et al. Enhancer-associated H3K4 monomethylation by Trithorax-related, the *Drosophila* homolog of mammalian Mll3/Mll4. *Genes Dev.* **26**, 2604–2620 (2012).
- Hu, D. et al. The MLL3/MLL4 branches of the COMPASS family function as major histone H3K4 monomethylases at enhancers. *Mol. Cell. Biol.* **33**, 4745–4754 (2013).
- Ang, S. Y. et al. KMT2D regulates specific programs in heart development via histone H3 lysine 4 di-methylation. *Development* **143**, 810–821 (2016).
- Lee, J. E. et al. H3K4 mono- and di-methyltransferase MLL4 is required for enhancer activation during cell differentiation. *Elife* **2**, e01503 (2013).
- Creyghton, M. P. et al. Histone H3K27ac separates active from poised enhancers and predicts developmental state. *Proc. Natl. Acad. Sci. USA* **107**, 21931–21936 (2010).
- Tie, F. et al. Trithorax monomethylates histone H3K4 and interacts directly with CBP to promote H3K27 acetylation and antagonize Polycomb silencing. *Development* **141**, 1129–1139 (2014).
- Wang, S. P. et al. A UTX-MLL4-p300 transcriptional regulatory network coordinately shapes active enhancer landscapes for eliciting transcription. *Mol. Cell* **67**, 308–321 (2017).
- Wang, C. et al. Enhancer priming by H3K4 methyltransferase MLL4 controls cell fate transition. *Proc. Natl. Acad. Sci. USA* **113**, 11871–11876 (2016).
- Lai, B. et al. MLL3/MLL4 are required for CBP/p300 binding on enhancers and super-enhancer formation in brown adipogenesis. *Nucleic Acids Res.* **45**, 6388–6403 (2017).
- Kim, D. H. et al. Crucial roles of mixed-lineage leukemia 3 and 4 as epigenetic switches of the hepatic circadian clock controlling bile acid homeostasis in mice. *Hepatology* **61**, 1012–1023 (2015).
- Phelps, C. J., Romero, M. I. & Hurley, D. L. Growth hormone-releasing hormone-producing and dopaminergic neurons in the mouse arcuate nucleus are independently regulated populations. *J. Neuroendocrinol.* **15**, 280–288 (2003).
- van den Pol, A. N. et al. Neuromedin B and gastrin-releasing peptide excite arcuate nucleus neuropeptide Y neurons in a novel transgenic mouse expressing strong Renilla green fluorescent protein in NPY neurons. *J. Neurosci.* **29**, 4622–4639 (2009).
- Cowley, M. A. et al. Leptin activates anorexigenic POMC neurons through a neural network in the arcuate nucleus. *Nature* **411**, 480–484 (2001).
- Xu, Q., Tam, M. & Anderson, S. A. Fate mapping Nkx2.1-lineage cells in the mouse telencephalon. *J. Comp. Neurol.* **506**, 16–29 (2008).
- Davis, A. M., Seney, M. L., Walker, H. J. & Tobet, S. A. Differential colocalization of Islet-1 and estrogen receptor alpha in the murine preoptic area and hypothalamus during development. *Endocrinology* **145**, 360–366 (2004).
- Dellovade, T. L. et al. Disruption of the gene encoding SF-1 alters the distribution of hypothalamic neuronal phenotypes. *J. Comp. Neurol.* **423**, 579–589 (2000).
- Lee, B. et al. Dlx1/2 and Otp coordinate the production of hypothalamic GHRH- and AgRP-neurons. *Nat. Commun.* **9**, 2026 (2018).
- Nasif, S. et al. Islet 1 specifies the identity of hypothalamic melanocortin neurons and is critical for normal food intake and adiposity in adulthood. *Proc. Natl. Acad. Sci. USA* **112**, E1861–E1870 (2015).
- Lee, B., Lee, S., Lee, S. K. & Lee, J. W. The LIM-homeobox transcription factor Isl1 plays crucial roles in the development of multiple arcuate nucleus neurons. *Development* **143**, 3763–3773 (2016).

37. McNay, D. E., Pelling, M., Claxton, S., Guillemot, F. & Ang, S. L. Mash1 is required for generic and subtype differentiation of hypothalamic neuroendocrine cells. *Mol. Endocrinol.* **20**, 1623–1632 (2006).
38. Bailey, T. L. et al. MEME SUITE: tools for motif discovery and searching. *Nucleic Acids Res.* **37**, W202–W208 (2009).
39. Machanick, P. & Bailey, T. L. MEME-ChIP: motif analysis of large DNA datasets. *Bioinformatics* **27**, 1696–1697 (2011).
40. Gupta, S., Stamatoyannopoulos, J. A., Bailey, T. L. & Noble, W. S. Quantifying similarity between motifs. *Genome Biol.* **8**, R24 (2007).
41. Kelly, D. P. & Scarpulla, R. C. Transcriptional regulatory circuits controlling mitochondrial biogenesis and function. *Genes Dev.* **18**, 357–368 (2004).
42. Quintana, F. J. et al. Control of T(reg) and T(H)17 cell differentiation by the aryl hydrocarbon receptor. *Nature* **453**, 65–71 (2008).
43. Bjornsson, H. T. et al. Histone deacetylase inhibition rescues structural and functional brain deficits in a mouse model of Kabuki syndrome. *Sci. Transl. Med.* **6**, 256ra135 (2014).
44. Lee, N. O. et al. TTF-1 regulates growth hormone and prolactin transcription in the anterior pituitary gland. *Biochem. Biophys. Res. Commun.* **362**, 193–199 (2007).
45. Lazzaro, D., Price, M., de Felice, M. & Di Lauro, R. The transcription factor TTF-1 is expressed at the onset of thyroid and lung morphogenesis and in restricted regions of the foetal brain. *Development* **113**, 1093–1104 (1991).
46. Price, M. et al. Regional expression of the homeobox gene Nkx-2.2 in the developing mammalian forebrain. *Neuron* **8**, 241–255 (1992).
47. Benjamin, J. S. et al. A ketogenic diet rescues hippocampal memory defects in a mouse model of Kabuki syndrome. *Proc. Natl. Acad. Sci. USA* **114**, 125–130 (2017).
48. Haberland, M., Montgomery, R. L. & Olson, E. N. The many roles of histone deacetylases in development and physiology: implications for disease and therapy. *Nat. Rev. Genet.* **10**, 32–42 (2009).
49. Lasko, L. M. et al. Discovery of a selective catalytic p300/CBP inhibitor that targets lineage-specific tumours. *Nature* **550**, 128–132 (2017).
50. Johnson, D. S., Mortazavi, A., Myers, R. M. & Wold, B. Genome-wide mapping of in vivo protein-DNA interactions. *Science* **316**, 1497–1502 (2007).
51. Robertson, G. et al. Genome-wide profiles of STAT1 DNA association using chromatin immunoprecipitation and massively parallel sequencing. *Nat. Methods* **4**, 651–657 (2007).

Acknowledgements

We are thankful to Dr. Kai Ge for kindly sharing *Mll4^{fl/fl}* mice with us. This work was supported by grants from NIH/NINDS (R01 NS111760 and R01 NS100471 to S.-K.L.) and NIH/NIDDK (R01 DK103661 to S.-K.L. and J.W.L.), by the Soongsil University Research Fund of 2018 (to S.K.), and by the National Research Foundation of Korea (NRF) grant funded by the Korea government (MSIT) (2019R1A2C2087068), Medical

Research Center (MRC) (NRF-2018R1A5A2024425) and a grant of the Korea Health Technology R&D Project through the Korea Health Industry Development Institute (KHIDI), funded by the Ministry of Health & Welfare, Republic of Korea (HI17C0447) (S.L.)

Author contributions

C.H., M.K.C., Y.A.K., S.J., B.S., J.C., and Y.P. designed and performed experiments and analyzed the data. S.J.L., S.M.Y., and S.K. analyzed the ChIP-seq data. S.L., S.-K.L., and J.L. directed the project and, together with C.H., wrote the paper. All authors discussed the results and commented on the manuscript.

Competing interests

The authors declare no competing interests.

Additional information

Supplementary information is available for this paper at <https://doi.org/10.1038/s41467-020-20511-7>.

Correspondence and requests for materials should be addressed to S.L. or J.W.L.

Peer review information *Nature Communications* thanks Alexandre Fiset, Lori Zeltser and Paolo Giacobini for their contribution to the peer review of this work.

Reprints and permission information is available at <http://www.nature.com/reprints>

Publisher's note Springer Nature remains neutral with regard to jurisdictional claims in published maps and institutional affiliations.



Open Access This article is licensed under a Creative Commons Attribution 4.0 International License, which permits use, sharing, adaptation, distribution and reproduction in any medium or format, as long as you give appropriate credit to the original author(s) and the source, provide a link to the Creative Commons license, and indicate if changes were made. The images or other third party material in this article are included in the article's Creative Commons license, unless indicated otherwise in a credit line to the material. If material is not included in the article's Creative Commons license and your intended use is not permitted by statutory regulation or exceeds the permitted use, you will need to obtain permission directly from the copyright holder. To view a copy of this license, visit <http://creativecommons.org/licenses/by/4.0/>.

© The Author(s) 2021